Hybrid electrostatic ion beam shepherd schemes for active space debris removal from GEO to disposal orbit

Alexander Ledkov (✉), **Vladimir Aslanov**

Theoretical Mechanics Department, Samara National Research University, Samara 443086, Russia

ABSTRACT

The removal of large space debris from a geostationary orbit to a disposal orbit via an ion beam shepherd spacecraft was considered in this study, with attention given to the electrostatic effect. The generation of an ion force, which provides contactless thrust, occurs because of the transfer of momentum from the ions of the engine plume of the spacecraft to the space debris. This process is accompanied by the transfer of a positive charge to the space debris. As a result, electrostatic interactions occur between the spacecraft and space debris. The goals of this study were to assess the influence of this effect on the dynamics of space debris during contactless ion beam-assisted removal and to develop hybrid contactless transportation schemes based on the use of an ion beam and electrostatic interactions. A mathematical model describing the motion of space debris and spacecraft under the influence of ionic and electrostatic forces and torques was developed. The concepts of electrostatic ion beam shepherd, electrostatic tractor with ion beam, and charged ion beam shepherd were proposed and compared. The results of numerical simulations revealed that the electrostatic ion beam shepherd scheme is preferable from the perspective of minimizing fuel costs when solving the problem of removing space debris from a geostationary orbit. A control law for the spacecraft charge needed for space-debris detumbling during ion-beam transportation is proposed. A numerical simulation of space debris removal was performed via a hybrid scheme.

KEYWORDS

space debris removal
ion beam shepherd (IBS)
electrostatic field
Coulomb force
orbital debris

Research Article

Received: 22 March 2024
Accepted: 2 July 2024

1 Introduction

Combining space debris threats is a complex and multifaceted task with great practical significance for the future use of space. One of the key measures is active space debris removal, which involves the use of an external spacecraft to move space debris to a disposal orbit or the boundary of the atmosphere with subsequent re-entry. In recent years, many different projects and methods have been proposed to implement active space debris removal missions. Their descriptions are available in Refs. [1–3]. On the basis of an analysis of these reviews, the methods for removing space debris can be divided into methods involving rigid capture or docking and subsequent transportation via a rigid link with a spacecraft, capture and subsequent transportation via a flexible tether, and contactless transportation. Among the proposed removal methods, contactless methods are the most promising. Safety is their main advantage because the absence of direct mechanical contact reduces the probability of accidents. The use of contactless methods significantly simplifies the implementation of multitarget missions, the importance of which has been emphasized by many researchers [4–6]. Several contactless methods have been proposed, including the use of electrostatic interactions [7], lasers [8], gravitational fields [9], and particle flows [10]. Methods based on electrostatic interactions involve charging space debris and spacecraft and using the Coulomb force to transport objects. Laser methods are based on the ablation effect, which generates

✉ ledkov@inbox.ru

Nomenclature

a_j^f	the j-th even coefficient of the expansion of function f in the Fourier series
b_j^f	the j-th odd coefficient of the expansion of function f in the Fourier series
C	integration constant
C_{M}	consistency matrix
c_j	gain coefficients (N, kg/s^2, kg/s)
d	distance between the center of mass of the space debris and spacecraft in transport mode (m)
$\boldsymbol{e}_{uj}$	unit vector directed along ion flow rate at the j-th triangle barycenter
$\boldsymbol{e}_{Nj}$	unit vector of the j-th triangle outer normal
F_A, F_B	resultant forces acting on points A and B (N)
F_{C}	Coulomb force (N)
F_{I}	ion force (N)
$F_{\mathrm{I}x}, F_{\mathrm{I}y}$	projections of ion force on the axes of the orbital reference frame (N)
F_{T}	thrust force of the impulse transfer and compensation engines (N)
g_0	Earth's gravitational acceleration near sea level (m/s^2)
h	self-similarity function
I_x, I_y, I_z	space debris moments of inertia (kg·m^2)
I_{sp}	specific impulse (s)
k_{C}	Coulomb's constant (Nm^2/C^2)
L_{C}	electrostatic torque (N·m)
L_{I}	ion torque (N·m)
l	distance between the centers of spheres simulating the charge of a cylinder (m)
m_A, m_B	spacecraft and space debris masses (kg)
m_i	mass of the ion (kg)
n_0	particle density at the beginning of far region (m^{-3})
n_j	particle density at the j-th triangle barycenter (m^{-3})
P_{C}	thrust force of compensation engines (N)
P_x, P_y	projections of resulting thrust force of all spacecraft engines on the axes of the orbital reference frame (N)
$\boldsymbol{Q}$	vector of charges of the spheres (C)
$\boldsymbol{q}$	vector of generalized coordinates
Q_A, Q_B	spacecraft and space debris charges (C)
Q_j^{g}	generalized force
q_i	charge of the i-th sphere (C)
q_j^{g}	generalized coordinate
R_0	ion beam radius at the beginning of the far region (m)
R_j	distance from the ion beam axis to the barycenter of the j-th triangle (m)
$R_{\mathrm{S}i}$	radius of the i-th sphere (m)
r	distance between the center of the Earth and the center of mass of space debris (m)
S_j	area of the j-th triangle (m^2)
T	kinetic energy (J)
U	potential energy (J)
u_0	ion velocity at the beginning of far region (m/s)
u_j	ion velocity at the j-th triangle barycenter (m/s)
u_{jr}	projection of ion velocity onto the ion beam axis (m/s)
u_{jz}	projection of ion velocity onto the direction perpendicular to the ion beam axis (m/s)
V_A, V_B	voltages on the spacecraft and space debris (V)
v_A, v_B	spacecraft and space debris velocities (m/s)
x, y	coordinates of a spacecraft in orbital reference frame (m)
x_A, y_A	coordinates of a spacecraft in inertial reference frame (m)
z_j	distance from the beginning of the ion beam far region to the projection of the j-th triangle barycenter onto the ion beam axis (m)
α	angle of deviation of the direction toward the spacecraft from the local horizontal of space debris (rad)
α_0	initial divergence angle of the 95% beam stream tube (rad)
β	angle between the ion beam axis and local horizon (rad)
ζ	dimensionless distance
η	momentum transfer efficiency coefficient
θ	angle of deviation of the axis of space debris from the local vertical line (rad)
μ	gravitational constant of the Earth (m^3/s^2)
ν	true anomaly angle of space debris (rad)
$\rho_{i,j}$	distance between the centers of the i-th and j-th spheres
$\boldsymbol{\rho}_j$	vector connecting space debris center of mass and center of the j-th sphere
$\boldsymbol{\Phi}$	voltage vector (V)

thrust when particles evaporate from a small area on the surface of space debris when they are melted by a laser. Gravity methods involve the use of a heavy collector station to attract space debris. Particle flow methods use the force generated on a space debris surface by the flow of particles emitted by a spacecraft that collide with the space debris. This study examined a hybrid method based on particle flow and electrostatic interactions.

Contactless space debris removal via particle flow is one of the methods that is the closest to practical implementation. It is assumed that a quasineutral plasma plume (ion beam) is generated by the electric propulsion thruster of an active spacecraft, which is located approximately 10 m from the space debris. This method of contactless exposure forms the basis of the ion beam shepherd (IBS) concept [10], which was developed by a group of researchers within the framework of an FP7 grant [11]. A shepherd spacecraft is equipped with two oppositely directed thrusters. One is used to generate a force on the space debris surface, and the second compensates for the thrust of the first to hold the spacecraft near the space debris (Fig. 1). An analysis of the technological feasibility of a space debris removal mission from low Earth orbit was conducted in Ref. [12]. This review highlights the main weaknesses and challenges faced by IBS projects. A preliminary design methodology for an IBS mission based on the matching chart approach is described in Ref. [13]. A more technically sound spacecraft design based on the Express-1000NV platform and an ion thruster with a divergence half-angle of 2° was provided in Ref. [14]. Theoretical and experimental results for the development of such thrusters are described in Ref. [15]. A previous study [16] showed that the attitude motion of space debris has a significant effect on the average ionic force generated during contactless transportation. Various methods and laws for controlling the attitude motion of space debris during ion transport are described in Section 5.3 of the monograph [17]. An ion beam can be used for detumbling space debris [18, 19]. Refs. [20, 21] were devoted to the development of control laws for active spacecraft during ion-beam-assisted transportation. The problems involved in using ion beams to remove space debris from a geostationary orbit (GEO) were considered in Ref. [22]. The results of an ion beam propagation analysis and the corresponding experimental data presented in this

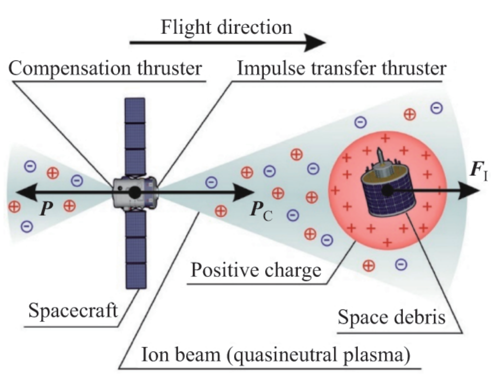

Fig. 1 Ion beam shepherd (IBS) concept for contactless space debris removal.

work confirmed the feasibility of generating the ion force required for the mission. One study [23] showed that one active spacecraft could use this noncontact method to remove up to 10 space debris objects from GEO.

When an ion beam interacts with the surface of space debris, various physical phenomena can occur, including surface sputtering, ion backscattering, and space debris charging. These phenomena were analyzed in Ref. [24] on the basis of the results of a numerical simulation via the EP2PLUS hybrid code [25]. According to the calculation results [24], when space debris is irradiated with an ion beam, it attains a positive charge of approximately 10 V relative to the spacecraft (Fig. 1). Because the Debye length in GEO exceeds 100 m, electrostatic interactions can occur between the charged spacecraft and space debris. The Coulomb force can be utilized to remove space debris from GEO.

A large body of research has been devoted to the use of electrostatic forces to transport space debris out of GEO. The idea of using electrostatic attraction for the contactless transport of space debris in GEO was first formulated in Ref. [7], where it was shown that an electrostatic tractor (ET) force would enable the transfer of 1000 kg of space debris to a disposal orbit in a few months. The proposed concept involves equipping an active spacecraft with a charged-particle gun to control the charge of the spacecraft and transfer the charge to space debris, as well as inertial thrusters to change the debris orbit. Geostationary orbital conditions allow the generation of an electrostatic tractor force on the order of several milli-Newtons at a distance between the spacecraft and the space debris object of tens of meters, with a potential level of 10 kV between them. The electrostatic attractive force tends to pull space debris toward the spacecraft, whereas the thrust of the inertial thrusters separates the spacecraft from the space debris. This allows the space debris to be transported. We call this transportation scheme the pulling electrostatic tractor concept (Fig. 2). If the space debris object and spacecraft have a charge of the same sign, an electrostatic repulsive force arises between them. In this case, electrostatic transport can be performed in the pushing mode (Fig. 3). A comparison of the pushing and pulling configurations in terms of their resulting performances, relative motion stabilities, and amounts of robustness to ET failure was performed in Ref. [26]. Their study demonstrated that a pulling configuration would create a larger electrostatic

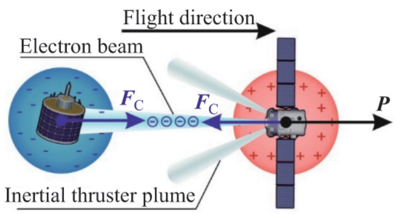

Fig. 2 Pulling electrostatic tractor concept for contactless space debris removal.

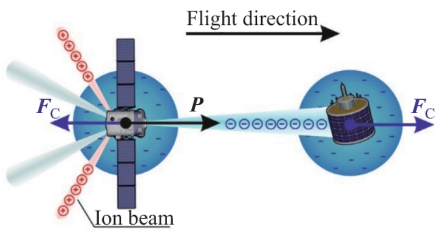

Fig. 3 Pushing electrostatic tractor concept for contactless space debris removal.

force at a given voltage. The authors also noted that the pulling configuration would be safe in the event of an ET failure. In Ref. [27], the pushing configuration was found to be safe in the event of a thruster failure, whereas a failure in the pulling configuration could result in a collision between the spacecraft and the debris object. The control law for the thrusters of an active spacecraft to ensure the asymptotic stability of its relative position when transporting a space debris object was also developed in this study for the pushing scheme. In Ref. [28], a control law for a spacecraft propulsion system that provides a fixed distance between the spacecraft and space debris was developed for the pulling scheme. Lyapunov's theory was used to prove the asymptotic stability of the controlled motion. The influence of local space weather on the controlled motion of a system was also studied in Ref. [29]. Weather had little effect on the pulling of the ET and could be compensated for by controlling the electron beam current.

The magnitude of the Coulomb force depends on the charges on the interacting bodies and the distance between them. The charges can change as a result of interactions with the environment. In particular, the charge on a body is affected by the thermal currents of plasma electrons and ions, secondary electron emission currents, backscattering currents, photoelectric effect currents, and ion or electron beam currents. A fairly detailed overview of these factors with reference to the main studies on the topic can be found in Ref. [30]. Charging models accounting for these effects can be found in Refs. [29, 31]. In Ref. [29], the effect of a geomagnetic storm on the performance of an electrostatic tractor was analyzed. This study revealed that the charge-transfer performance could be improved by using an ion gun along with an electron gun. The photoelectric current caused by sunlight has a significant influence on the charge on a body in GEO. It was noted in Ref. [32] that the natural potential of a body, which in turn affects currents and, through them, charges, reaches several positive volts when the body is under the Sun's rays, with a kilovolt-level negative potential in an eclipse. Various approaches can be used to determine the Coulomb force and electrostatic torque acting on a body. The multisphere method represents a body as a set of spheres, the sizes and locations of which are determined such that the electrostatic field generated by these spheres approaches the field obtained via a more accurate finite element model [33].

Electrostatic torque can be used to solve the problem of detumbling space debris objects. A previous review [34] provided a fairly complete picture of the problem of detumbling a space debris object and possible approaches to solve it on the basis of the use of electrostatic torque. The control law for the potential of a spacecraft, which provides stabilization of the angular oscillations of a space debris object in a planar case, was developed in Ref. [35] via Lyapunov theory. The results of this study were further developed in Ref. [36] for the three-dimensional case of an axisymmetric space debris object. In Ref. [37], Lyapunov's theory was used to prove that the control developed in Ref. [36] provides asymptotic stability during the push or pull transportation of space debris. Another control law for the electrostatic potential in a planar case was developed in Ref. [38]. In contrast to Ref. [35], this study considered a wider class of rate-feedback modulation functions; however, only the pushing configuration was investigated.

This study simultaneously considered the impact of an ion beam and the electrostatic effect on contactless space debris transportation. The goals of this study were to assess the influence of this effect on the dynamics of space debris during contactless ion beam-assisted removal and to develop a hybrid contactless transportation scheme based on the use of an ion beam and electrostatic interactions. The concepts described below include the development and synergy of the IBS and ET concepts.

Notably, the influence of the momentum transmitted by a charged particle flow to space debris, together with the electrostatic force of attraction, was first considered within the framework of the electrostatic tractor concept in a previous study [39]. This study revealed that electron beams are much more efficient than ion beams for electrostatic transport missions. However, there are system configurations in which the electrostatic force exceeds the repulsive force caused by the thrust of the ion gun and the transfer of momentum by the ions.

Three hybrid concepts were investigated in this study: electrostatic ion beam shear (EIBS), charged ion beam shepherd (CIBS), and electrostatic tractor with ion beam (ETIB). In the first concept, the spacecraft and space debris are positively charged, and an electrostatic repulsion force exists between them. In the other two concepts, the spacecraft is negatively charged, and the space debris is positively charged; therefore, an electrostatic attraction force acts between them. In all the cases, the ion beam generates an ionic force. In the first two concepts, the ionic force accelerates the space debris, and in the last concept, this force decelerates it. The possibility of using a charged ion beam rather than quasineutral plasma to generate an ionic force is of interest. In other words, the impulse-transfer thruster is an ion gun. This allows the transfer of positive charges to the space debris.

The remainder of this paper is organized as follows. Section 2 describes the mathematical model of a mechanical system comprising a spacecraft and space debris in the presence of ionic and electrostatic interactions between them. Methods for calculating the ion and electrostatic forces and torques are also described. Section 3 provides detailed descriptions of the proposed hybrid concepts. Section 4 presents the results of the numerical simulations, provides the system parameters, compares the hybrid transportation schemes, and proposes a spacecraft voltage control law to stabilize space debris oscillations. Section 5 presents the main conclusions of the study.

2 Mathematical model

2.1 Equations of motion

Consider the planar motion of a mechanical system consisting of an active spacecraft and a space debris object. The spacecraft is considered to be mass point A, and the space debris is a rigid body, with its center of mass located at point B (Fig. 4). The position of the space debris center of mass is given by the true anomaly angle, ν, and the distance to the center of the Earth, r. The angular position of the space debris is determined by the angle, θ. The position of the spacecraft relative to the space debris is given by its x and y coordinates in the orbital Cartesian reference frame BX_oY_o. It is assumed that the impulse transfer and compensation thrusters are installed on a rotating platform, which is controlled by an electric motor. This makes it possible to change the direction of the ion beam axis within certain limits without the need to reorient the spacecraft. The spacecraft control system estimates the position of the space debris and directs the axis of the ion beam toward the space debris center of mass. Thus, the state of the mechanical system is determined by five generalized coordinates: $\boldsymbol{q} = [\nu, r, \theta, x, y]^{\mathrm{T}}$, where $\boldsymbol{q}$ is the generalized coordinate vector. The ion force generated by the ion beam is specified by projections of the axes of the orbital coordinate system ($F_{\mathrm{I}x}$, $F_{\mathrm{I}y}$), whereas the Coulomb force F_{C} is directed along line AB. Figure 4 shows the resulting thrust force of all the spacecraft engines by projections P_x and P_y on the axes of the orbital coordinate system. The ion torque L_{I} and electrostatic torque L_{C} act on the space debris object and are shown in Fig. 4.

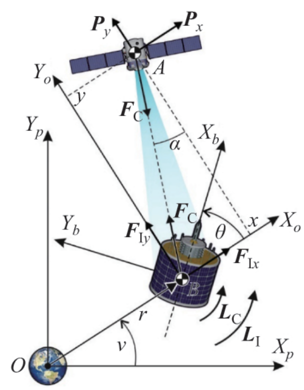

Fig. 4 Space debris and active spacecraft.

The Lagrange formalism was used to obtain the equations of motion of the mechanical system shown in Fig. 4. The kinetic energy of a mechanical system consisting of both the spacecraft and space debris has the form in Eq. (1):

$$T = \frac{m_A v_A^2}{2} + \frac{m_B v_B^2}{2} + \frac{I_z(\dot{\nu} + \dot{\theta})^2}{2} \tag{1}$$

where m_A and m_B are the spacecraft and debris object masses, respectively; $v_A = \sqrt{\dot{x}_A + \dot{y}_A}$ and $v_B = \sqrt{r^2\dot{\nu}^2 + \dot{r}^2}$ are the spacecraft and debris object velocities, respectively; and I_z is the transverse moment of inertia of the space debris. To calculate the spacecraft velocity, we determine the coordinates of point A in the inertial coordinate system OX_pY_p.

$$\begin{cases} x_A = (r+x)\cos\nu - y\sin\nu \\ y_A = (r+x)\sin\nu + y\cos\nu \end{cases} \tag{2}$$

By calculating the derivatives of these coordinates and substituting the results into Eq. (1), the expression in Eq. (3) for the kinetic energy is obtained:

$$\begin{aligned} T = {} & \frac{m_A[(r+x)^2 + y^2]\dot{\nu}^2 + (\dot{r}+\dot{x})^2 + \dot{y}^2}{2} \\ & + \frac{2[(r+x)\dot{y} - y(\dot{r}+\dot{x})]\dot{\nu}}{2} + \frac{m_B(r^2\dot{\nu}^2 + \dot{r}^2)}{2} \\ & + \frac{I_z(\dot{\nu}+\dot{\theta})^2}{2} \end{aligned} \tag{3}$$

The potential energy of the central gravitational field for the mechanical system considered has the form in Eq. (4):

$$\begin{aligned} U = {} & -\frac{\mu m_A}{\sqrt{x_A^2 + y_A^2}} - \frac{\mu m_B}{r} - \frac{\mu(I_x + I_y + I_z)}{2r^3} \\ & + \frac{3\mu(I_x\cos^2\theta + I_y\sin^2\theta)}{2r^3} \end{aligned} \tag{4}$$

where μ is the gravitational constant of the Earth and I_x and I_y are the principal moments of inertia of the space debris object. The Lagrange equations of the second type can be written as Eq. (5):

$$\frac{\mathrm{d}}{\mathrm{d}t}\frac{\partial T}{\partial \dot{q}_j^{\mathrm{g}}} - \frac{\partial T}{\partial q_j^{\mathrm{g}}} = -\frac{\partial U}{\partial q_j^{\mathrm{g}}} + Q_j^{\mathrm{g}} \tag{5}$$

where q_j^{g} is a component of the vector of the generalized coordinates, $\boldsymbol{q}$, and Q_j^{g} is the corresponding generalized force.

$$\begin{aligned} & Q_\nu^{\mathrm{g}} = F_{\mathrm{I}y}r - P_x y + P_y(r+x) - \delta F_{\mathrm{C}} x\cos\alpha + L_{\mathrm{I}} + L_{\mathrm{C}}, \\ & Q_r^{\mathrm{g}} = F_{\mathrm{I}x} + P_x, \quad Q_r^{\mathrm{g}} = L_{\mathrm{I}} + L_{\mathrm{C}}, \\ & Q_x^{\mathrm{g}} = P_x - \delta F_{\mathrm{C}}\sin\alpha, \quad Q_y^{\mathrm{g}} = P_y - \delta F_{\mathrm{C}}\cos\alpha \end{aligned} \tag{6}$$

Here, $\delta = -\mathrm{sign}(Q_A Q_B)$ is the coefficient determining the direction of the Coulomb forces; Q_A and Q_B are the spacecraft and space debris charges, respectively; and α is the angle of deviation of the direction toward the spacecraft from the local horizontal of the space debris.

$$\sin\alpha = \frac{x}{\sqrt{x^2+y^2}}, \quad \cos\alpha = \frac{y}{\sqrt{x^2+y^2}} \tag{7}$$

Substituting Eqs. (3), (4), and (6) into Eq. (5) and expressing the second derivatives from the resulting system of equations, we obtain

$$\begin{aligned} \ddot{r} = {} & \dot{\nu}^2 r - \frac{\mu}{r^2} + \frac{F_{\mathrm{I}x} + \delta F_{\mathrm{C}}\sin\alpha}{m_B} \\ & + \frac{3\mu(3I_x\cos^2\theta + 3I_y\sin^2\theta - I_x - I_y + I_z)}{2m_B r^4} \end{aligned} \tag{8}$$

$$\ddot{\nu} = -\frac{2\dot{\nu}\dot{r}}{r} + \frac{F_{\mathrm{I}y} + \delta F_{\mathrm{C}}\cos\alpha}{m_B r} - \frac{3\mu(I_x - I_y)\sin\theta\cos\theta}{m_B r^5} \tag{9}$$

$$\begin{aligned} \ddot{\theta} = {} & \frac{L_{\mathrm{I}} + L_{\mathrm{C}}}{I_z} + \frac{2\dot{\nu}\dot{r}}{r} - \frac{F_{\mathrm{I}y} + \delta F_{\mathrm{C}}\cos\alpha}{m_B r} \\ & + \frac{3\mu(I_x - I_y)\sin\theta\cos\theta}{I_z r^3} \end{aligned} \tag{10}$$

$$\begin{aligned} \ddot{x} = {} & \ddot{\nu}y - \ddot{r} + \dot{\nu}^2(r+x) + 2\dot{\nu}\dot{y} + \frac{P_x - \delta F_{\mathrm{C}}\sin\alpha}{m_A} \\ & - \frac{\mu(r+x)}{[(r+x)^2 + y^2]^{3/2}} \end{aligned} \tag{11}$$

$$\begin{aligned} \ddot{y} = {} & \dot{\nu}^2 y - \ddot{\nu}(r+x) - 2\dot{\nu}(\dot{r}+\dot{x}) + \frac{P_y - \delta F_{\mathrm{C}}\cos\alpha}{m_A} \\ & - \frac{\mu y}{[(r+x)^2 + y^2]^{3/2}} \end{aligned} \tag{12}$$

The resulting system of differential equations (8)–(12) is in close agreement with the equations obtained in Ref. [40] for the IBS scheme. Unlike the system described in that study, electrostatic forces and torques are added to the right-hand sides of the equations. In addition, in Eq. (10), the term $1/(m_B r^2)$ is neglected because $I_z \ll m_B r^2$.

The spacecraft is located at a point with coordinates $x = 0$ and $y = -d$ to transfer space debris from the protected GEO region to a higher disposal orbit. Simple PD control can cope with the task of holding a spacecraft in this relative position:

$$P_x = -c_x x - c_{dx}\dot{x}, \; P_y = c_{y0} + c_y(-d - y) - c_{dy}\dot{y} \tag{13}$$

where are gain coefficients. Equation (14) is used to calculate fuel costs:

$$\dot{m}_{\mathrm{f}} = \frac{2F_{\mathrm{T}} + |P_x| + |P_y|}{I_{\mathrm{sp}} g_0} \tag{14}$$

where F_{T} is the thrust force of the impulse transfer and compensation engines, I_{sp} is the specific impulse, and $g_0 = 9.80665\mathrm{m/s}^2$ is the Earth's gravitational acceleration near sea level.

2.2 Ion force and torque calculation

The calculation procedure described in Refs. [17] and [41] was used to obtain the ion force F_{I} and torque L_{I}. This was based on a simplified self-similar model for plasma propagation. In this procedure, the surface of a space debris object is divided into triangles, and the force generated by the plasma plume for each triangle is calculated. A self-similar model is used to determine the plasma parameters around each triangle. After the forces for all the triangles were calculated, the resulting force and torque about the center of mass were calculated. According to Ref. [17], the ionic force acting on the j-th triangle can be calculated as Eq. (15):

$$\boldsymbol{F}_{\mathrm{I}j} = -n_j m_i S_j u_j^2 \boldsymbol{e}_{uj} (\boldsymbol{e}_{uj} \cdot \boldsymbol{e}_{Nj}) \tag{15}$$

where n_j is the ion particle density at the barycenter of the j-th triangle, m_i is the ion mass, S_j is the area of the j-th triangle, u_j is the ion velocity at the barycenter of the j-th triangle, $\boldsymbol{e}_{uj}$ is a unit vector directed along the ion flow rate at the barycenter of the j-th triangle, and $\boldsymbol{e}_{Nj}$ is the unit vector of the outer normal of the j-th triangle. The particle density can be determined as Eq. (16) [41]:

$$n_j = \frac{n_0}{h(\zeta)^2} \exp\left(-C \frac{R_j^2}{2R_0^2 h(\zeta)^2}\right) \tag{16}$$

where R_j is the distance from the ion beam axis to the barycenter of the j-th triangle (Fig. 5); $\zeta = z_j/R_0$ is the dimensionless distance; z_j is the distance from the beginning of the ion beam far region to the projection of the barycenter of the j-th triangle onto the ion beam axis; R_0 is the ion beam radius at the beginning of the far region ($z_j = 0$); n_0 is the plasma density at the beginning of the far region; $h(\zeta) = 1 + \zeta \tan \alpha_0$ is the self-similarity function; α_0 is the initial divergence angle of the 95% beam stream tube; and $C \approx 6$ is an integration constant [41]. The far region is a conventionally defined zone of the ion beam that begins at a distance of several R_0 radii from the beam source, and simplified models of plasma propagation can be used. The velocity vector, $\boldsymbol{u}_j = u_j \boldsymbol{e}_{uj}$, lies in the plane formed by the ion beam axis and barycenter of the j-th triangle. It is assumed that the projection of the velocity onto the ion beam axis, $u_{jz} = u_0$, does not depend on the coordinates of the considered point, and the component perpendicular to it, u_{jr}, is determined by the similarity function:

$$u_{jr} = u_0 \frac{R_j}{R_0} \frac{h'(\zeta)}{h(\zeta)} \tag{17}$$

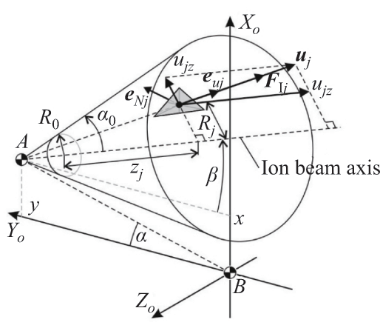

Fig. 5 Ion beam geometry.

The ion force and torque depend on the ion beam parameters, relative position of the spacecraft, and direction of the ion beam axis. For the considered plane case, it is convenient to represent the ion force and torque in the form of a Fourier series expansion as Eqs. (18)–(20):

$$F_{\mathrm{I}x} = a_0^{F_{\mathrm{I}x}} + \sum_{j=1}^{k} (a_j^{F_{\mathrm{I}x}} \cos j\theta + b_j^{F_{\mathrm{I}x}} \sin j\theta) \tag{18}$$

$$F_{\mathrm{I}y} = a_0^{F_{\mathrm{I}y}} + \sum_{j=1}^{k} (a_j^{F_{\mathrm{I}y}} \cos j\theta + b_j^{F_{\mathrm{I}y}} \sin j\theta) \tag{19}$$

$$L_{\mathrm{I}} = a_0^{L_{\mathrm{I}}} + \sum_{j=1}^{k} (a_j^{L_{\mathrm{I}}} \cos j\theta + b_j^{L_{\mathrm{I}}} \sin j\theta) \tag{20}$$

where $a_j^f = a_j^f(x, y, \beta)$ and $b_j^f = b_j^f(x, y, \beta)$ are Fourier series expansion coefficients, which are functions of coordinates x and y, and the direction of the ion beam axis given by the angle β (Fig. 5). For the axis of the ion beam to be directed toward the center of mass of the space debris, $\beta = -\alpha$. When the mathematical model developed in Section 2.1 is used, it is advisable to perform a preliminary calculation of the coefficients of Eqs. (18)–(20) for a space debris object with a given shape and then use these values to obtain coefficients corresponding to the current position of the spacecraft and orientation of the space debris via interpolation. The Fourier series approximation is actively used in numerical simulations of ion beam space debris removal missions [17, 40].

2.3 Electrostatic force and torque calculations

The volume multisphere method [33] was used to calculate the electrostatic force and torque. In this method, the charge distribution of an object is modeled via a set of conductive spheres located inside it (Fig. 6). It is assumed that the radii of these spheres and their locations inside the object are predetermined via various optimization techniques [42, 43] and do not change during system motion. This method assumes that the voltages on the spacecraft (V_A) and space debris (V_B) are known. In practical implementations, the equipment for measuring

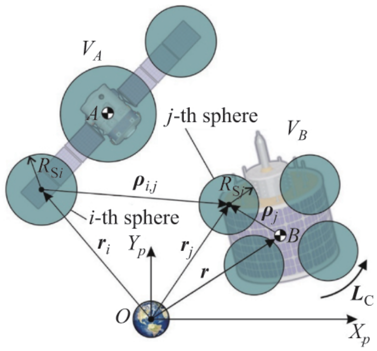

Fig. 6 Multisphere method geometry sample.

the voltage on noncooperative space debris should be installed on an active spacecraft. Various remote-sensing methods for space debris potential have been described [44]. Another study [45] proposed a hybrid method for determining the surface voltage of a remote object on the basis of the observation of X-rays and spectra emitted from the surface electrons of the object. The voltage matrix $\boldsymbol{\Phi}$ is a columnar matrix whose first N_A rows correspond to the spacecraft, with the next N_B rows corresponding to the space debris.

$$\boldsymbol{\Phi} = [\overbrace{V_A, \cdots, V_A}^{N_A}, \overbrace{V_B, \cdots, V_B}^{N_B}]^{\mathrm{T}} \tag{21}$$

This voltage matrix is used to calculate the charges of the spheres, q_i. The charge vector $\boldsymbol{Q} = [\overbrace{q_1, \cdots, q_{N_A}}^{N_A}, \overbrace{q_{N_A+1}, \cdots, q_{N_A+N_B}}^{N_B}]^{\mathrm{T}}$ can be found as Eq. (22):

$$\boldsymbol{Q} = \frac{1}{k_{\mathrm{C}}} C_{\mathrm{M}} \boldsymbol{\Phi} \tag{22}$$

where $k_{\mathrm{C}} = 8.99 \times 10^9\ \mathrm{N{\cdot}m^2/C^2}$ is Coulomb's constant and C_{M} is the capacitance matrix:

$$[C_{\mathrm{M}}]^{-1} = \begin{bmatrix} 1/R_{\mathrm{S1}} & 1/\rho_{1,2} & \cdots & 1/\rho_{1,N-1} & 1/\rho_{1,N} \\ 1/\rho_{2,1} & 1/R_{\mathrm{S2}} & \ddots & \vdots & \vdots \\ \vdots & \ddots & \ddots & \vdots & \vdots \\ 1/\rho_{N-1,1} & \cdots & \cdots & 1/R_{\mathrm{S}N-1} & 1/\rho_{N-1,N} \\ 1/\rho_{N,1} & \cdots & \cdots & 1/\rho_{N,N-1} & 1/R_{\mathrm{S}N} \end{bmatrix} \tag{23}$$

where $N = N_A + N_B$; R_{S1} is the radius of the i-th sphere; and $\rho_{i,j} = |\boldsymbol{r}_j - \boldsymbol{r}_i|$ is the distance between the centers of the i-th and j-th spheres, as specified by the radius vectors $\boldsymbol{r}_i$ and $\boldsymbol{r}_j$ (Fig. 6). The coordinates of these vectors change during system motion. This leads to redistribution of the charges between the spheres. After the charges are calculated, the Coulomb force can be determined as Eq. (24):

$$\boldsymbol{F}_{\mathrm{C}} = \delta k_{\mathrm{C}} \sum_{i=1}^{N_A} \sum_{j=N_A+1}^{N} \frac{q_i q_j \boldsymbol{\rho}_{i,j}}{\rho_{i,j}^3} \tag{24}$$

and the electrostatic torque acting on the space debris from the spacecraft can be found as Eq. (25):

$$\boldsymbol{L}_{\mathrm{C}} = \delta k_{\mathrm{C}} \sum_{i=1}^{N_A} \sum_{j=N_A+1}^{N} \frac{q_i q_j}{\rho_{i,j}^3} \boldsymbol{\rho}_j \times \boldsymbol{\rho}_{i,j} \tag{25}$$

where $\boldsymbol{\rho}_j$ is the vector connecting point B to the center of the j-th sphere. The electrostatic force and torque depend on the relative position of the spacecraft and space debris, as well as their angular orientation.

3 Hybrid electrostatic ion beam shepherd schemes

3.1 Electrostatic ion beam shepherd

In the electrostatic ion beam shepherd (EIBS) scheme (Fig. 7), the space debris and spacecraft are charged with the same sign. The resulting Coulomb force, F_{C}, repels the space debris from the spacecraft and is codirected with the ion force F_{I}. The compensation thruster, which keeps the spacecraft near the space debris, must compensate not only for the thrust force P of the impulse transfer thruster but also for the Coulomb force acting on the spacecraft, F_{C} (Fig. 7). The advantage of this scheme is that the Coulomb force increases the resulting touch-less force acting on the space debris.

3.2 Charged ion beam shepherd

The charged ion beam shepherd (CIBS) scheme (Fig. 8) differs from the EIBS scheme in that the spacecraft and space debris have charges with opposite signs and are attracted to each other. The generated ion force prevails over the Coulomb force; therefore, a compensation thruster that creates force P_{C} is required to keep the spacecraft near the debris. Notably, the proposed scheme differs from the classic electrostatic tractor concept in the pull configuration, which was described and analyzed

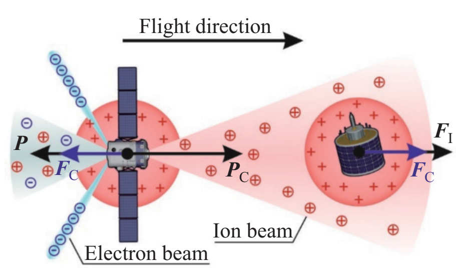

Fig. 7 Electrostatic ion beam shepherd concept (EIBS).

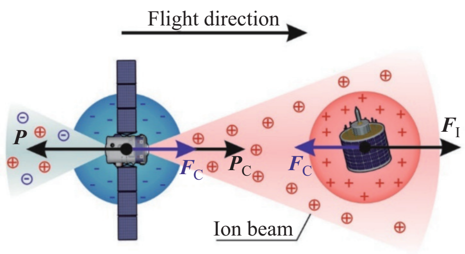

Fig. 8 Charged ion beam shepherd (CIBS) concept.

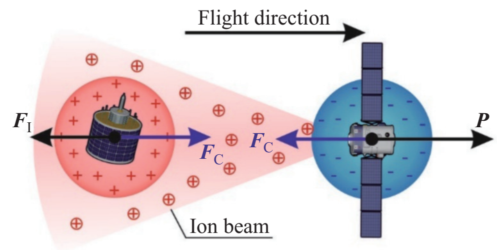

Fig. 9 Electrostatic tractor with ion beam (ETIB) concept.

in a previous study [26]. The key difference is the use of the ion force and electrostatic repulsion for transport purposes. The influence of the ionic force is fundamental to the proposed scheme. Schaub and Jasper [26] did not consider the force created by the flow of particles transferring a charge and the possibility of using it in a positive way.

3.3 Electrostatic tractor with ion beam

The electrostatic tractor with ion beam (ETIB) scheme (Fig. 9) is based on the attraction force between oppositely charged bodies. This is a modification of the electrostatic tractor concept [31], which involves the use of an electron or ion gun to transfer charges and two inertial engines to create thrust. The key difference in the proposed scheme is the use of a single-ion thruster to give the space debris a positive charge and create the thrust of the spacecraft. A portion of the ion beam can pass through space debris without participating in charge transfer or ion force generation. Because ions that collide with the surface of space debris generate an ion force, F_{I}, in the opposite direction to the attractive Coulomb force, F_{C}, a balance between the distance between the space debris and spacecraft, the divergence angle of the ion beam, and the thrust generated during beam creation, P, must be found to achieve contactless transportation.

4 Numerical simulation results

4.1 Mechanical system parameters

As an example, consider the removal of a hypothetical cylindrical satellite from GEO to a disposal orbit. The center of mass of the cylinder coincides with its geometric center. The length of the cylinder is 3 m, and its radius is 0.5 m. The masses of the spacecraft and space debris are assumed to be $m_A = 500$ kg and $m_B = 1000$ kg, respectively. These cylinder dimensions were chosen because they were used in a previous study [33] to calculate the parameters of a system of equivalent spheres via the multisphere method. The space debris moments of inertia are $I_x = 250$ kg·m^2 and $I_y = I_z = 750$ kg·m^2. The gain coefficients of the spacecraft's thrusters are $c_x = c_y = 1000$ kg/s^2, $c_{dx} = c_{dy} = 1000$ kg/s, and $c_{y0} = -0.0062$ N.

The calculations of the position and size of an equivalent system of spheres to simulate the charge of such a cylinder are given in a previous paper [33]. According to the data given there, the spacecraft is represented as one sphere, $N_A = 1$, and the space debris is modeled as three spheres, $N_B = 3$. In the body-fixed coordinate system, $BX_bY_bZ_b$ (Fig. 4, where the Z_b axis is perpendicular to the plane of the figure and directed toward us), vectors defining the positions of the spheres have the following coordinates: $\boldsymbol{\rho}_2^b = [l, 0, 0]^{\mathrm{T}}$, $\boldsymbol{\rho}_3^b = [0, 0, 0]^{\mathrm{T}}$, $\boldsymbol{\rho}_4^b = [-l, 0, 0]^{\mathrm{T}}$, and $l = 1.1454$ m. The radii of the spheres are $R_{\mathrm{S1}} = 1$ m, $R_{\mathrm{S2}} = R_{\mathrm{S4}} = 0.5959$ m, and $R_{\mathrm{S3}} = 0.6534$ m. The spacecraft is assumed to be located at a distance of $d = 7$ m from the space debris. To calculate the Coulomb force and electrostatic torque via the procedure described in Section 2.3, the vectors must be converted to the orbital coordinate system: $\boldsymbol{\rho}_1^o = [x, y, 0]^{\mathrm{T}}$, $\boldsymbol{\rho}_2^o = [l\cos\theta, l\sin\theta, 0]^{\mathrm{T}}$, $\boldsymbol{\rho}_3^o = [0, 0, 0]^{\mathrm{T}}$, and $\boldsymbol{\rho}_4^o = [-l\cos\theta, l\cos\theta, 0]^{\mathrm{T}}$. The capacitance matrix C_{M}, which is used to calculate the charges, depends on the coordinates of the spacecraft $(x,\, y)$ and the space debris orientation angle θ. The dependence of the Coulomb force on the angle θ is shown in Fig. 10 for the EIBS and ETIB schemes. Figure 11 shows the corresponding dependences of the electrostatic torque. A potential value of ± 30 kV for the spacecraft and space debris was selected on the basis of the examples discussed in previous papers [7, 31, 33, 43] to demonstrate the features of the hybrid transportation schemes under consideration.

The graphs in Figs. 10 and 11 show that with the same voltage modulus, the attractive electrostatic force is greater than the repulsive force, and the amplitude

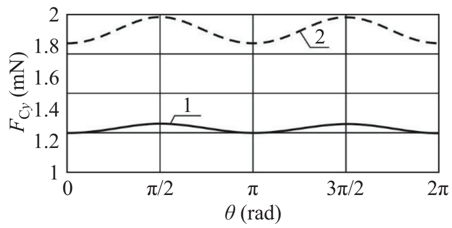

Fig. 10 Coulomb force for (1) $V_A = V_B = -30$ kV, $x = 0$, and $y = -7$ m (EIBS) and (2) $V_A = 30$ kV, $V_B = -30$ kV, $x = 0$, and $y = 7$ m (ETIB).

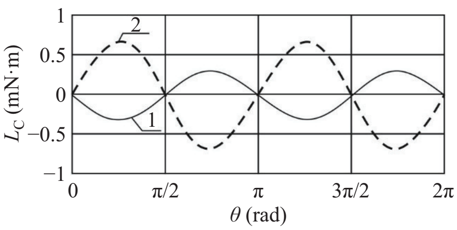

Fig. 11 Electrostatic torque for (1) $V_A = V_B = -30$ kV, $x = 0$, and $y = -7$ m (EIBS) and (2) $V_B = 30$ kV, $V_B = -30$ kV, $x = 0$, and $y = 7$ m (ETIB).

of the electrostatic torque in the case of attraction is greater than that in the case of repulsion. This behavior is consistent with the results of a previous study [26].

The spacecraft is assumed to be equipped with a NASA evolutionary xenon thruster commercial gridded ion thruster [46]. The thruster has a specific impulse $I_{\mathrm{sp}} = 4155$ s and creates thrust $F_{\mathrm{T}} = 0.235$ N. The evaluation formulas given in Section 4.2 of monograph [17] make it possible to calculate the following parameters of the ion beam on the basis of the characteristics of the thruster: $u_0 = 40{,}747$ m/s, $n_0 = 6.3787 \times 10^{15}$ m^{-3}, $m_i = 2.18 \times 10^{-25}$ kg, $\alpha_0 = 10°$, $R_0 = 0.18$ m, and $\dot{m} = 5.7673 \times 10^{-6}$ kg/s. Figures 11 and 12 show the dependence of the projections of the ion force and torque for the case where the spacecraft is located at a point with coordinates $x = 0$ and $y = 7$ m. For the case where the coordinate $y < 0$, the projections of the ion force and torque can be found as Eq. (26):

$$\begin{cases} F_{\mathrm{I}x}(\theta, x, y) = F_{\mathrm{I}x}(-\theta, x, -y) \\ F_{\mathrm{I}y}(\theta, x, y) = -F_{\mathrm{I}y}(-\theta, x, -y) \\ L_{\mathrm{I}}(\theta, x, y) = -L_{\mathrm{I}}(-\theta, x, -y) \end{cases} \tag{26}$$

Because of the symmetry of the ion-beam flow pattern around the cylinder. Here, the right side of the above equations is obtained for the case of $y > 0$, and these forces and torques are shown in Figs. 12–14. Because of the symmetry of the beam particles blowing through the cylinder, the force projection $F_{\mathrm{I}z}$ is equal to zero.

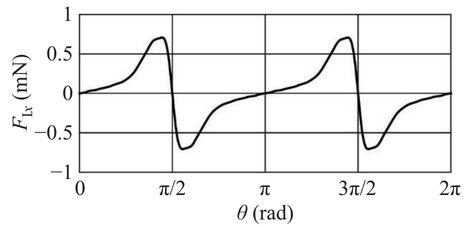

Fig. 12 Ion force projection $F_{\mathrm{I}x}$ for $x = 0$ and $y = 7$ m.

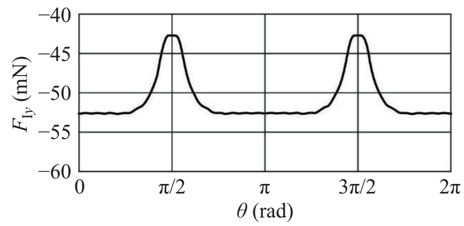

Fig. 13 Ion force projection $F_{\mathrm{I}y}$ for $x = 0$ and $y = 7$ m.

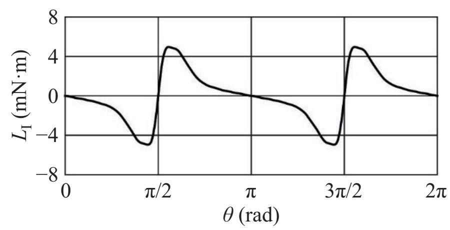

Fig. 14 Ion torque for $x = 0$ and $y = 7$ m.

A comparison of Figs. 10, 13, 11, and 14 shows that for the considered mechanical system, the ion force and torque are an order of magnitude greater than the electrostatic forces. Therefore, the ion beam has a dominant influence on the dynamics of the system. The graphs of the ion and electrostatic torques have the same zero values (Figs. 11 and 14). The nature of the change in the ion torque graph is similar to that of the change in the electrostatic torque for the EIBS scheme and has an antiphase relationship with the electrostatic torque for the CIBS and ETIB schemes. This implies that under deep-space conditions, when there is no effect from the gravitational gradient and inertial moments, a more complex angular behavior will be observed in the cases of the CIBS and ETIB schemes. The counteraction of the ion and electrostatic torques leads to the emergence of new equilibrium positions near the $\pi n/2$ points, where $n \in \mathbb{Z}$ occurs.

4.2 Comparison of hybrid contactless transport schemes

We consider a simplified one-dimensional formulation of the contactless transportation problem to evaluate the effectiveness of the proposed hybrid schemes. In addition to the IBS, the EIBS and ETIB schemes described in Section 3 were evaluated. Two mass points, A and B, move along a straight line under the influence of forces P, P_{C}, F_{I}, and F_{C} (Fig. 15):

$$m_A \ddot{x}_A = F_A \tag{27}$$

$$m_B \ddot{x}_B = F_B \tag{28}$$

where F_A and F_B are projections of the resultant forces onto the X-axis for points A and B respectively, and the distance, d, between points remains constant during transportation; thus, $\ddot{x}_A = \ddot{x}_B$. Let us determine the scheme for which the sum of the modules of thrust forces P and P_{C} is minimal for a given value of the resultant force F_B. This scheme requires the lowest fuel consumption for transportation. The impulse transfer engine thrust force P and generated ion force F_{I} are assumed to be related by the expression in Eq. (29):

$$F_{\mathrm{I}} = \eta P \tag{29}$$

where $\eta \in (0, 1)$ denotes the momentum transfer efficiency coefficient. Let us determine the resultant force, F_B, for each scheme (Fig. 15) and express the thrust force P accordingly. The results are presented in the second and third columns of Table 1. To determine force P_{C}, it is necessary to express $\ddot{x}_B$ from Eq. (28) and substitute

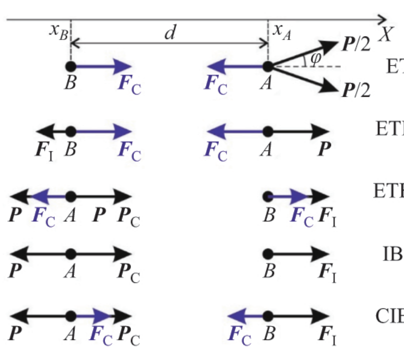

Fig. 15 One-dimensional representation of transportation schemes.

it into Eq. (27), considering $\ddot{x}_A = \ddot{x}_B$. The results are presented in the fourth column of Table 1. The last column lists the total engine thrust. Table 1 is sorted in ascending order of the last column. In addition to the hybrid concepts, Table 1 and Fig. 15 contain the classic IBS and ET schemes in a pulling configuration. Angle φ refers to the angle of deviation of the axes of the inertial thrusters of an ET.

Let us take a closer look at the process of filling out the table, using the row for the EIBS scheme as an example. According to Fig. 15, the resulting forces at points A and B can be written as Eqs. (30) and (31):

$$F_A = P_{\mathrm{C}} - P - F_{\mathrm{C}} \tag{30}$$

$$F_B = F_{\mathrm{I}} + F_{\mathrm{C}} \tag{31}$$

The right-hand side of Eq. (31) is written in the second column of the table. Substituting Eq. (29) into Eq. (31) and expressing the force P yields

$$P = \frac{F_B - F_{\mathrm{C}}}{\eta} \tag{32}$$

These values are listed in the third column of Table 1. Let us express the derivatives of Eqs. (27) and (28) and equate them, taking into account Eq. (30):

$$\frac{P_{\mathrm{C}} - P - F_{\mathrm{C}}}{m_A} = \frac{F_B}{m_B} \tag{33}$$

The expression for P_{C} from Eq. (33) gives

$$P_{\mathrm{C}} = F_B \frac{m_A}{m_B} + F_{\mathrm{C}} + P \tag{34}$$

Considering Eq. (32), the last expression can be rewritten as Eq. (35):

$$P_{\mathrm{C}} = F_B \left(\frac{m_A}{m_B} + \frac{1}{\eta} \right) - F_{\mathrm{C}} \left(\frac{1}{\eta} - 1 \right) \tag{35}$$

This value is listed in the fourth column of Table 1. The values of P_{C} and P are positive because $F_B > F_{\mathrm{C}}$ for the considered scheme. Summing Eqs. (32) and (35) yields

$$P + P_{\mathrm{C}} = F_B \left(\frac{m_A}{m_B} + \frac{2}{\eta} \right) - F_{\mathrm{C}} \left(\frac{2}{\eta} - 1 \right) \tag{36}$$

This value is written in the fifth column of Table 1.

Table 1 Comparison of forces across schemes

	F_B	P	P_{C}	$\lvert P\rvert + \lvert P_{\mathrm{C}}\rvert$
ET	F_{C}	$\frac{F_B}{\cos\varphi}\left(\frac{m_A}{m_B}+1\right)$	0	$\frac{F_B}{\cos\varphi}\left(\frac{m_A}{m_B}+1\right)$
ETIB	$F_{\mathrm{C}} - F_{\mathrm{I}}$	$F_B\frac{m_A}{m_B} + F_{\mathrm{C}}$	0	$F_B\frac{m_A}{m_B} + F_{\mathrm{C}}$
EIBS	$F_{\mathrm{C}} + F_{\mathrm{I}}$	$\frac{F_B - F_{\mathrm{C}}}{\eta}$	$F_B\left(\frac{m_A}{m_B}+\frac{1}{\eta}\right) - F_{\mathrm{C}}\left(\frac{1}{\eta}-1\right)$	$F_B\left(\frac{m_A}{m_B}+\frac{2}{\eta}\right) - F_{\mathrm{C}}\left(\frac{2}{\eta}-1\right)$
IBS	F_{I}	$\frac{F_B}{\eta}$	$F_B\left(\frac{m_A}{m_B}+\frac{1}{\eta}\right)$	$F_B\left(\frac{m_A}{m_B}+\frac{2}{\eta}\right)$
CIBS	$F_{\mathrm{I}} - F_{\mathrm{C}}$	$\frac{F_B + F_{\mathrm{C}}}{\eta}$	$F_B\left(\frac{m_A}{m_B}+\frac{1}{\eta}\right) + F_{\mathrm{C}}\left(\frac{1}{\eta}-1\right)$	$F_B\left(\frac{m_A}{m_B}+\frac{2}{\eta}\right) + F_{\mathrm{C}}\left(\frac{2}{\eta}-1\right)$

An analysis of the results given in Table 1 shows that the ETIB scheme is the most effective from the point of view of minimizing the required total engine thrust. However, for practical implementation, it is necessary that $F_{\mathrm{C}} > F_{\mathrm{I}}$. Otherwise, the spacecraft will be unable to drag space debris. Fulfilling this condition requires a large potential difference between the spacecraft and space debris. A comparison of Figs. 10 and 13 reveals that for the example under consideration, this scheme is unrealizable because $F_{\mathrm{C}} < F_{\mathrm{I}}$ ($\max(|F_{\mathrm{I}}|) = 0.052$ N, $\max(|F_{\mathrm{I}}|) = 0.003$ N). The least effective scheme is the CIBS scheme, in which the spacecraft and space debris have charges of opposite signs and are attracted to each other. To achieve the required level for the transport force F_B, additional fuel is required to compensate for the attractive force at point B.

Numerical simulations of space debris removal from GEO to a disposal orbit via the mathematical model developed in Section 2 were performed for the IBS, CIBS, and EIBS contactless transportation schemes. The initial conditions in Eq. (37) were used in the simulations:

$$\begin{aligned}&r_0 = 42{,}164{,}000\ \mathrm{m},\ \dot{r}_0 = 0\ \mathrm{m/s},\ \nu_0 = 0\ \mathrm{rad},\\&\dot{\nu}_0 = 7.2922\times10^{-5}\ \mathrm{rad/s},\ \theta_0 = 0.3\ \mathrm{rad},\ \dot{\theta}_0 = 0\ \mathrm{rad/s},\\&x_0 = 0\ \mathrm{m},\ \dot{x}_0 = 0\ \mathrm{m/s},\ y_0 = -7\ \mathrm{m},\ \dot{y}_0 = 0\ \mathrm{m/s}\end{aligned} \tag{37}$$

The radius of the disposal orbit is $r_{\mathrm{d}} = 42{,}414{,}000$ m, which is 250 km greater than the GEO radius. For the EIBS scheme, the potentials of the spacecraft and space debris were $V_A = V_B = -30$ kV. For the CIBS scheme, $V_A = 30$ kV and $V_B = -30$ kV were used. Figure 16 shows the space debris radius as a function of time for the various schemes. The standard IBS scheme would allow a spacecraft to remove space debris in $t_{\mathrm{IBS}} = 45.87$ h. In this case, the mass of fuel consumed would be $m_{\mathrm{IBS}} = 2.010$ kg. In the EIBS case, transportation is faster ($t_{\mathrm{EIBS}} = 42.91$ h) and requires less fuel ($m_{\mathrm{EIBS}} = 1.889$ kg). The simulation in the case of the CIBS scheme revealed that if the spacecraft and space debris acquired large charges with different signs during transportation by the ion beam, then the transportation time ($t_{\mathrm{CIBS}} = 54.29$ h) and fuel consumption ($m_{\mathrm{CIBS}} = 2.360$ kg) increased. In particular, in the considered case, the fuel consumption increased by 17%.

The fuel calculation described above does not consider the costs of generating and maintaining charges on the spacecraft and space debris. The classic electrostatic pulling tractor with an electron beam is more fuel efficient than the hybrid concepts analyzed in this study. However, its main disadvantage compared with the IBS and hybrid concepts is the relatively small value of the Coulomb force with which transportation is performed. This results in a multifold increase in the time required to complete the mission.

4.3 Space debris oscillation

Although the electrostatic torque is several times smaller than the ion torque, it can have a significant effect on the mode of angular oscillations of a space debris object. Figure 17 shows the results of the numerical integration of the system of Eqs. (8)–(12) with the parameters given in Section 4.2. When the CIBS scheme is used, the oscillations of the space debris are very different from the results obtained for the IBS and EIBS schemes, which are associated with the superposition of the ion and electrostatic torques. According to Eq. (10), the determining influence on space debris oscillations is exerted by the ion (L_{I}), electrostatic (L_{C}), and gravity gradient (L_{G}) torques, where

$$L_{\mathrm{G}} = \frac{3\mu(I_x - I_y)\sin\theta\cos\theta}{I_z r^3} \tag{38}$$

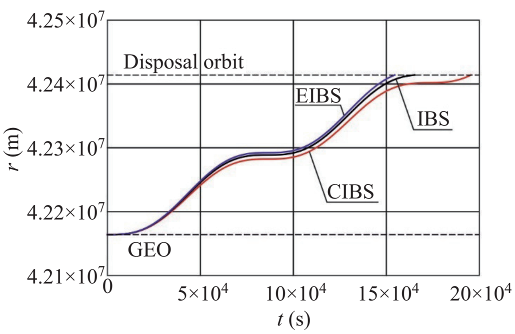

Fig. 16 Dependence of the space debris radius on time.

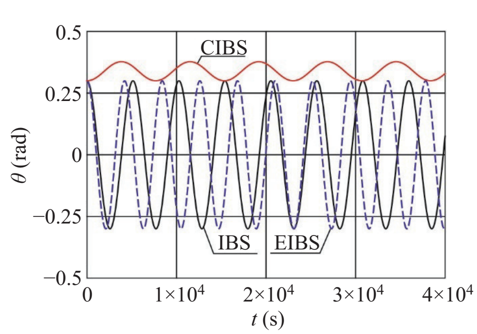

Fig. 17 Dependence of angle θ on time.

Figure 18 shows the dependences of the resulting torque, $L = L_{\mathrm{I}} + L_{\mathrm{C}} + L_{\mathrm{G}}$, on the angle θ for the IBS, EIBS, and CIBS schemes for r = 42,164,000 m. The intersection of this moment graph with the x-axis corresponds to the equilibrium position. In the EIBS case, the addition of an electrostatic torque does not lead to the appearance of additional equilibrium positions. Therefore, the oscillations shown in Fig. 17 occur around $\theta = 0$. In the CIBS case, four new stable equilibrium positions appear near point $\theta = 0$, and the point itself becomes unstable. Figure 17 shows that in this case, oscillations occur around a stable equilibrium position, $\theta = 0.343$ rad.

4.4 Electrostatic detumbling during ion-beam-assisted transportation

Electrostatic torque can be used to solve the problem of detumbling and stabilizing the angular motion of space debris during ion-beam-assisted transportation. An EIBS scheme is considered. Considering the features of the ion (Fig. 14) and electrostatic torques (Fig. 11), the relay control of the spacecraft voltage in Eq. (39) can be proposed:

$$V_A = -V_{A0} H(\dot{\theta}\theta) \tag{39}$$

where $V_{A0} = 30$ kV and H is the Heaviside theta function. This control is based on the concept of directing the electrostatic torque in the opposite direction to the direction of rotation of the space debris. If it turns out to be codirected with the direction of the current rotation, then it is zeroed as a result of the zeroing of potential V_A. Figure 19 shows the dependence of the space-debris deflection angle θ on time. The gray line shows the graph corresponding to the uncontrolled case when $V_A = -30$ kV. The proposed control solves the problem of stabilizing space debris at the equilibrium position $\theta = 0$. The corresponding voltage is shown in Fig. 20. Consider in more detail the operation of the control law specified by Eq. (39) for one period of oscillation of angle θ. In the graph for section AB, the angular velocity $\dot{\theta}$ is negative, and the angle θ is positive. Thus, their product has a negative value, and the Heaviside function in Eq. (39) returns a value of zero. If there was no control, the electrostatic moment would accelerate the oscillations in this area. Angle θ changes sign at point B. Thus, the Heaviside function changes its value to one. The electrostatic torque in section BC is directed in the opposite direction to the angular velocity and slows down the angular oscillations. Angle θ reaches a minimum at point C. At this point, the angular velocity $\dot{\theta}$ changes sign and becomes positive. The Heaviside function again takes a value of zero. Angle θ changes sign at point D, and the Heaviside function at section DE takes a value of one. Thus, in sections BC and DE, the electrostatic torque slows the angular oscillations.

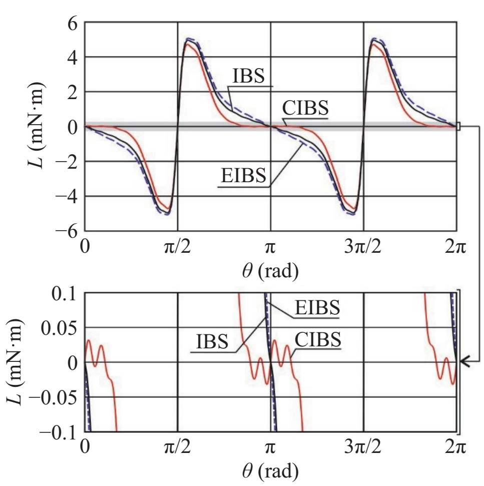

Fig. 18 Dependence of the resulting torque $L = L_{\mathrm{I}}+L_{\mathrm{C}}+L_{\mathrm{G}}$ on the angle θ.

5 Conclusions

In this study, hybrid schemes for contactless space debris

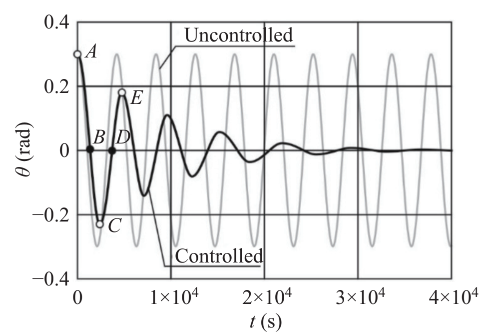

Fig. 19 Dependence of angle θ on time for $V_A = -30$ kV (gray line) and control of Eq. (39) (black line).

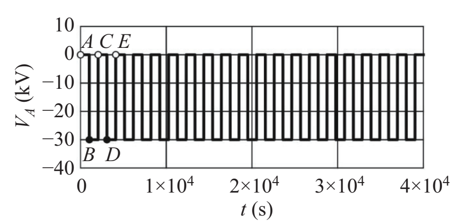

Fig. 20 Dependence of the voltage control of Eq. (39) on time.

transportation were proposed and analyzed. A system of equations describing the plane motion of a mechanical system consisting of a spacecraft and space debris under the influence of gravitational, ionic, and electrostatic forces and torques was obtained. Numerical simulations of space debris removal from a GEO were performed.

The classic electrostatic pulling tractor with an electron beam is more fuel efficient than the hybrid concepts analyzed in this study. However, its main disadvantage compared with the IBS and hybrid concepts is its relatively small Coulomb force, which results in a multifold increase in the space debris removal mission time. The ETIB scheme was found to be the most effective hybrid scheme from the point of view of minimizing the required engine thrust; however, its practical implementation requires that the Coulomb attraction force exceeds the generated ion force, which may require the generation of large potentials on the spacecraft and space debris. The presence of Coulomb attraction between the space debris and spacecraft (the CIBS scheme), with the predominance of the ion force, reduces the efficiency of ion beam-assisted transportation, which is expressed as increases in the transportation time and fuel cost. The presence of a Coulomb repulsion force between the spacecraft and space debris during ion transportation (the EIBS scheme) increases the transportation efficiency, which is expressed as decreases in the mass of the required fuel and transportation time. The presence of an electrostatic torque can have a significant effect on the mode of angular oscillation of space debris during ion transport. Electrostatic torque can be used to control the angular motion of space debris during ion transport. The possibility of stabilizing space debris in an equilibrium position through relay control of the active spacecraft voltage was demonstrated.

Notably, the conducted research was the first step toward the development of hybrid contactless transportation schemes. It is necessary to conduct careful studies on the possibility of transferring and conserving an electrostatic charge in the presence of the quasineutral plasma flow that makes up an ion beam. Exploring the possibility of modifying engines to use a charged ion beam to transfer a charge to space debris within the framework of ion-beam-assisted transportation would be interesting. In addition, the presence of charged bodies can affect the operation of an engine, the generation of an ion beam, and the nature of the ion beam propagation itself.

Acknowledgements

This study was supported by the Russian Science Foundation (Project No. 22-19-00160, https://rscf.ru/en/project/22-19-00160/).

Declaration of competing interest

The authors have no competing interests to declare that are relevant to the content of this article.

References

[1] Aslanov, V. S., Ledkov, A. S. Survey of tether system technology for space debris removal missions. *Journal of Spacecraft and Rockets*, **2023**, 60(5): 1355–1371.

[2] Mark, C. P., Kamath, S. Review of active space debris removal methods. *Space Policy*, **2019**, 47: 194–206.

[3] Shan, M. H., Guo, J., Gill, E. Review and comparison of active space debris capturing and removal methods. *Progress in Aerospace Sciences*, **2016**, 80: 18–32.

[4] Wijayatunga, M. C., Armellin, R., Holt, H., Pirovano, L., Lidtke, A. A. Design and guidance of a multi-active debris removal mission. *Astrodynamics*, **2023**, 7(4): 383–399.

[5] Baranov, A. A., Grishko, D. A. Review of path planning in prospective multi-target active debris removal missions in low earth orbits. *Progress in Aerospace Sciences*, **2024**, 145: 100982.

[6] Medioni, L., Gary, Y., Monclin, M., Oosterhof, C., Pierre, G., Semblanet, T., Comte, P., Nocentini, K. Trajectory optimization for multi-target active debris removal missions. *Advances in Space Research*, **2023**, 72(7): 2801–2823.

[7] Schaub, H., Moorer, D. F. Geosynchronous large debris reorbiter: Challenges and prospects. *The Journal of the Astronautical Sciences*, **2012**, 59(1): 161–176.

[8] Phipps, C. R., Bonnal, C. A spaceborne, pulsed UV laser system for re-entering or nudging LEO debris, and re-orbiting GEO debris. *Acta Astronautica*, **2016**, 118: 224–236.

[9] Aslanov, V. S. Debris removal in GEO by heavy orbital collector. *Acta Astronautica*, **2019**, 164: 184–191.

[10] Bombardelli, C., Pelaez, J. Ion beam shepherd for contactless space debris removal. *Journal of Guidance, Control, and Dynamics*, **2011**, 34(3): 916–920.

[11] Ruiz, M., Urdampilleta, I., Bombardelli, C., Ahedo, E., Merino, M., Cichocki, F. The FP7 LEOSWEEP project: Improving low earth orbit security with enhanced electric propulsion. In: Proceedings of the Space Propulsion Conference, **2014**: 35–42.

[12] Colpari, R., Sajjad, N., Kiran, A., Chakraborty, M., Tripathi, V., Baranwal, P., Janardhana, B., Stepanova,

D., Wischert, D. Conceptual analysis for a technology demonstration mission of the ion beam shepherds. *CEAS Space Journal*, **2023**, 15(4): 567–584.

[13] Urrutxua, H., Bombardelli, C., Hedo, J. M. A preliminary design procedure for an ion-beam shepherd mission. *Aerospace Science and Technology*, **2019**, 88: 421–435.

[14] Obukhov, V. A., Kirillov, V. A., Petukhov, V. G., Popov, G. A., Svotina, V. V., Testoyedov, N. A., Usovik, I. V. Problematic issues of spacecraft development for contactless removal of space debris by ion beam. *Acta Astronautica*, **2021**, 181: 569–578.

[15] Melnikov, A. V., Bogachev, E. A., Elakov, A. B., Mogulkin, A. I., Obukhov, V. A., Perminova, Y., Peysakhovich, O. D., Pokrishkin, A. I., Svotina, V. V., Cherkasova, M. V. Computational and experimental study of an ion injector of a weakly divergent ion beam for implementing a method for removing space debris objects by an ion beam. *Acta Astronautica*, **2023**, 204: 815–825.

[16] Ledkov, A. S. Determining the effective space debris attitude motion modes for ion-beam-assisted transportation. *Journal of Spacecraft and Rockets*, **2024**, 61(1): 104–113.

[17] Aslanov, V., Ledkov, A. *Attitude Dynamics and Control of Space Debris During Ion Beam Transportation*. Elsevier, **2023**.

[18] Zhao, H. Q., Dai, H. H. Optimal detumbling guidance and control of plasma plume for tumbling spacecraft. *Nonlinear Dynamics*, **2024**, 112(6): 4465–4482.

[19] Nakajima, Y., Tani, H., Mitani, S., Yamamoto, T. Efficiency improving guidance for detumbling of space debris using thruster plume impingement. In: Proceedings of the IEEE Aerospace Conference, **2020**: 1–12.

[20] Obukhov, V. A., Kirillov, V. A., Petukhov, V. G., Pokryshkin, A. I., Popov, G. A., Svotina, V. V., Testoyedov, N. A., Usovik, I. V. Control of a service satellite during its mission on space debris removal from orbits with high inclination by implementation of an ion beam method. *Acta Astronautica*, **2022**, 194: 390–400.

[21] Alpatov, A., Khoroshylov, S., Bombardelli, C. Relative control of an ion beam shepherd satellite using the impulse compensation thruster. *Acta Astronautica*, **2018**, 151: 543–554.

[22] Kitamura, S., Hayakawa, Y., Kawamoto, S. A reorbiter for large GEO debris objects using ion beam irradiation. *Acta Astronautica*, **2014**, 94(2): 725–735.

[23] Nikolichev, I. A., Svotina, V. V. Contactless space debris removal from the geostationary orbit protected region. *Acta Astronautica*, **2024**, 215: 523–533.

[24] Cichocki, F., Merino, M., Ahedo, E. Spacecraft-plasma-debris interaction in an ion beam shepherd mission. *Acta Astronautica*, **2018**, 146: 216–227.

[25] Cichocki, F., Domínguez-Vázquez, A., Merino, M., Ahedo, E. Hybrid 3D model for the interaction of plasma thruster plumes with nearby objects. *Plasma Sources Science and Technology*, **2017**, 26(12): 125008.

[26] Schaub, H., Jasper, L. E. Z. Orbit boosting maneuvers for two-craft coulomb formations. *Journal of Guidance, Control, and Dynamics*, **2013**, 36(1): 74–82.

[27] Aslanov, V., Yudintsev, V. Motion control of space tug during debris removal by a coulomb force. *Journal of Guidance, Control, and Dynamics*, **2018**, 41(7): 1476–1484.

[28] Hogan, E. A., Schaub, H. Relative motion control for two-spacecraft electrostatic orbit corrections. *Journal of Guidance, Control, and Dynamics*, **2013**, 36(1): 240–249.

[29] Hogan, E. A., Schaub, H. Space weather influence on relative motion control using the touchless electrostatic tractor. *The Journal of the Astronautical Sciences*, **2016**, 63(3): 237–262.

[30] Bengtson, M., Wilson, K., Hughes, J., Schaub, H. Survey of the electrostatic tractor research for reorbiting passive GEO space objects. *Astrodynamics*, **2018**, 2(4): 291–305.

[31] Hogan, E. A., Schaub, H. Impacts of tug and debris sizes on electrostatic tractor charging performance. *Advances in Space Research*, **2015**, 55(2): 630–638.

[32] Lai, S. T. *Fundamentals of Spacecraft Charging: Spacecraft Interactions with Space Plasmas*. Princeton University Press, **2012**.

[33] Stevenson, D., Schaub, H. Multi-Sphere Method for modeling spacecraft electrostatic forces and torques. *Advances in Space Research*, **2013**, 51(1): 10–20.

[34] Bennett, T., Stevenson, D., Hogan, E., Schaub, H. Prospects and challenges of touchless electrostatic detumbling of small bodies. *Advances in Space Research*, **2015**, 56(3): 557–568.

[35] Schaub, H., Stevenson, D. Prospects of relative attitude control using coulomb actuation. *The Journal of the Astronautical Sciences*, **2013**, 60(3): 258–277.

[36] Bennett, T., Schaub, H. Touchless electrostatic three-dimensional detumbling of large axi-symmetric debris. *The Journal of the Astronautical Sciences*, **2015**, 62(3): 233–253.

[37] Bennett, T., Schaub, H. Contactless electrostatic detumbling of axi-symmetric GEO objects with nominal pushing or pulling. *Advances in Space Research*, **2018**, 62(11): 2977–2987.

[38] Aslanov, V., Schaub, H. Detumbling attitude control analysis considering an electrostatic pusher configuration. *Journal of Guidance, Control, and Dynamics*, **2019**, 42(4): 900–909.

[39] Schaub, H., Sternovsky, Z. Active space debris charging for contactless electrostatic disposal maneuvers. *Advances in Space Research*, **2014**, 53(1): 110–118.

[40] Aslanov, V. S., Ledkov, A. S., Konstantinov, M. S. Attitude motion of a space object during its contactless ion beam transportation. *Acta Astronautica*, **2021**, 179: 359–370.

[41] Alpatov, A., Cichocki, F., Fokov, A., Khoroshylov, S., Merino, M., Zakrzhevskii, A. Determination of the force transmitted by an ion thruster plasma plume to an orbital object. *Acta Astronautica*, **2016**, 119: 241–251.

[42] Ingram, G., Hughes, J., Bennett, T., Reilly, C., Schaub, H. Volume multi-sphere-model development using electric field matching. *The Journal of the Astronautical Sciences*, **2018**, 65(4): 377–399.

[43] Stevenson, D., Schaub, H. Optimization of sphere population for electrostatic multi-sphere method. *IEEE Transactions on Plasma Science*, **2013**, 41(12): 3526–3535.

[44] Bengtson, M. T., Schaub, H. Remote sensing of spacecraft potential at geosynchronous orbit using secondary and photo electrons. In: Proceedings of the AIAA Scitech Forum, **2019**: AIAA 2019-0311.

[45] Wilson, K., Bengtson, M., Schaub, H. Hybrid method of remote sensing of electrostatic potential for proximity operations. In: Proceeding of the IEEE Aerospace Conference, **2020**: 1–9.

[46] Fisher, J., Ferraiuolo, B., Monheiser, J., Goodfellow, K., Hoskins, A., Myers, R., Bontempo, J., McDade, J., O'Malley, T., Soulas, G., Shastry, R., Gonzalez, M. NEXT-C flight ion system status. In: Proceedings of the AIAA Propulsion and Energy Forum, **2020**: AIAA 2020-3604.

Alexander Ledkov received his Ph.D. degree in theoretical mechanics from Samara State Aerospace University (Russia) in 2009. Since 2009, he has worked as an associate professor in the Theoretical Mechanics Department at Samara National Research University and holds a joint appointment as a senior researcher at the Mechanics Research Laboratory at the same university. His research interests include classical mechanics, mechanics of space flight, dynamics of tethered satellite systems, contactless transport in space, and reentry vehicle dynamics. He is the coauthor of "*Dynamics of the Tethered Satellite System*" and *"Attitude Dynamics and Control of Space Debris During Ion Beam Transportation*", published by Elsevier.

Vladimir Aslanov has been a professor at Samara National Research University since 1989. From 2019 to 2021, he also served as the head of the Space Flight Mechanics Laboratory at the Moscow Aviation Institute. His scientific interests include classical mechanics, nonlinear oscillations and chaotic dynamics, mechanics of space flight, dynamics of gyrostats, and dynamics of tethered satellite systems and spacecraft stability. He has published multiple books, including "*Dynamics of Tethered Satellite Systems*", "*Rigid Body Dynamics for Space Dynamics*", and "*Attitude Dynamics and Control of Space Debris During Ion Beam Transportation*", all with Elsevier.